RSC Advances

PAPER

View Article Online
View Journal | View Issue

Cite this: *RSC Adv.*, 2017, **7**, 21398

Protein adsorption and desorption behavior of a pH-responsive membrane based on ethylene vinyl alcohol copolymer

Hui Ye,[ab] Lilan Huang,[ab] Wenrui Li,[ab] YuZhong Zhang,*[ab] Lizhi Zhao,[ab] Qingping Xin,[ab] Shaofei Wang,[ab] Ligang Lin[ab] and Xiaoli Ding[ab]

Received 18th March 2017
Accepted 7th April 2017

DOI: 10.1039/c7ra03206d

rsc.li/rsc-advances

Protein adsorption and desorption behavior was investigated for a pH-responsive ethylene vinyl alcohol copolymer (EVAL) membrane with an interconnected porous structure. The transition of electrostatic behavior and conformation change of the poly(dimethylaminoethyl methacrylate) (poly(DMAEMA)) chain contributed to the pH-responsive protein adsorption and desorption. Protein adsorption was conducted under acidic and neutral conditions. Protein desorption was conducted under alkaline conditions. The protonated poly(DMAEMA) chain was positively charged and extended into the BSA solution below its pK_a, providing a three-dimensional space for BSA adsorption. The maximum static protein adsorption capacity was obtained at pH 6.4. The dynamic adsorption capacities of membrane $EVAL_{10}$ at 10% and 50% breakthrough were 45 and 99 mg BSA per g of membrane, respectively. The $Q_{50\%}$ of membrane $EVAL_{10}$ was equivalent to 22.6 mg BSA per mL of membrane, almost 95% of the static adsorption capacity. BSA was quickly desorbed from the membrane and 94% recovery of BSA was observed at pH 9.0 in the dynamic desorption process, due to a deprotonated and collapsed conformation of the poly(DMAEMA) chains. The dynamic adsorption capacity of the membrane did not change significantly after four sequential cycles.

1. Introduction

The conventional resin-based chromatography used for protein recovery and purification has several major limitations, *e.g.*, high-pressure drop and long process time. Membrane chromatography, which makes use of a microporous membrane as chromatographic support material, is considered to have a lower pressure drop, higher processing speed and higher throughput process than resin-based chromatography. A predominantly convective transport mechanism of the solutes through the membrane pores to the adsorption sites is superior to the intraparticle diffusion transport mechanism of resin-based chromatography. Until now, various types of membranes have been investigated for protein purification,[1,2] *i.e.*, membrane chromatography based on ion exchange,[3–6] affinity,[7–9] and hydrophobic interactions.[10,11]

Stimuli-responsive membrane can change structural and functional properties (*i.e.* pore-size, porosity, surface charge and hydrophilicity) in response to environment conditions such as temperature, pH, electric or magnetic field and ionic strength.[12–14] Recently, there is an increased interest in the stimuli-responsive surfaces which can change their affinity towards biomolecules under external stimuli.[15–17] Raja Ghosh *et al.*[18] prepared the hydrogel-paper composite membranes for temperature-responsive protein recovery by hydrophobic interaction membrane chromatography. The hydrophobic or hydrophilic states of membranes could be regulated by the addition or removal of salts for selective antibody binding. Subsequently, Raja Ghosh *et al.*[11] fabricated temperature-responsive membrane by grafting poly-(*N*-isopropyl acrylamide) (PNIPAM) onto filter paper surface. The protein binding could be controlled for temperature-based separation. However, the salt- and temperature-responsive membranes possibly led to certain problems and challenges, such as high pressure drop and deposition of salts within equipment in the salt-based mode, or protein stability problems in the temperature-based mode. The pH-responsive membranes can be potentially useful for selective bio-separation, but very few developments on pH-responsive membranes for protein purification have been reported up to now.

Poly(dimethylaminoethyl methacrylate) (poly(DMAEMA)) is a weak cationic polyelectrolyte with tertiary amine groups, which can ionize under alkaline conditions (pK_a 8.5–9.5). The degree of ionization of weak polyelectrolytes can be flexibly adjusted by pH value, thus the weak polyelectrolytes seem more favorable to control electrostatic interactions between weak polyelectrolytes and feed solutes compared to strong polyelectrolytes.[19] The poly(DMAEMA) has been employed for preparing ion exchange, antimicrobial and pH-responsive

[a]*State Key Laboratory of Separation Membranes and Membrane Processes, Tianjin Polytechnic University, Tianjin 300387, China. E-mail: zhangyz2004cn@163.com; Fax: +86-22-83955806; Tel: +86-22-83955810*

[b]*School of Materials Science and Engineering, Tianjin Polytechnic University, Tianjin 300387, China*

membrane, but studies to develop protein separation performance based on the electrostatic behavior and conformation change of poly(DMAEMA) are still limited. Moreover, the permeability and selectivity of pH-responsive membranes grafted with poly(DMAEMA) chains can be regulated at high pH, which could be potential application for separating mixtures containing alkaline components, *e.g.* soy protein concentrates,[20,21] whey protein concentrates[22,23] and traditional Chinese medicine (TCM) extracts.[24,25]

Ethylene vinyl alcohol copolymer (EVAL) is a promising biomedical material with excellent hydrophilicity and biocompatibility.[26,27] Incorporation of hydroxy groups increases the wettability of membrane and reduces the non-selective (irreversible) adsorption between the biomolecules and the membrane surface, especially in protein separation.[28,29] To our knowledge, the protein separation performance of EVAL membrane functionalized with grafted pH-responsive polymers has not yet been reported.

The pH-responsive EVAL ultrafiltration membrane has been reported in an earlier paper from our group.[30,31] The pH-responsive properties of the poly(DMAEMA)-grafted EVAL membrane were observed in the pH range of 9–10, but the surface of the membrane was dense. Such dense surface had a negative impact on convective transport and led to protein rejection. In the present study, the protein adsorption and desorption behavior was investigated for a pH-responsive EVAL membrane prepared by grafting DMAEMA onto EVAL microfiltration membrane. The effective surface charge characteristic of membrane in response to pH was measured. Protein adsorption measurements (BSA as model protein) were used to evaluate the pH-responsive protein separation of the membranes. The protein adsorption and desorption were investigated in dynamic process and the effect of flow rate on dynamic adsorption was studied.

2. Experimental

2.1 Materials

EVAL (ethylene content of 44 mol%) was purchased from Kuraray (Japan). Dimethylsulfoxide (DMSO) (solvent) and 1-octanol (non-solvent additive) were purchased from Tianjin Guangfu Chemical Reagent Co. Ltd. (China). DMAEMA (98%) was purchased from J&K Chemicals (Beijing, China) and was purified under depressurized condition to remove the inhibitor before usage. BSA (molecular weight of 68 kDa) was sourced from Sigma-Aldrich. Benzophenone (BP) purchased from TCI (Shanghai) Development Co. Ltd was used as photoinitiator. The sodium dihydrogen phosphate (NaH_2PO_4), sodium hydrogen phosphate (Na_2HPO_4), hydrochloric acid (HCl) and sodium hydroxide (NaOH) were used of analytical reagent grade and obtained from Tianjin Fengchuan Chemical Reagent Co. Ltd. (China).

2.2 Preparation of original EVAL membrane

The microfiltration EVAL membrane with high pore interconnectivity was used as porous support. Such original EVAL membrane was prepared by phase inversion method.[32] 15 wt% EVAL polymer and 20 wt% of 1-octanol were dissolved in 65 wt% DMSO at 70 °C and ultrasonicated for 30 min to eliminate bubbles. Solutions were cast on a glass plate, and immersed in a water bath at 40 °C until fully cured. After that, the membranes were taken out and washed by ethanol to remove remaining solvent and additive.

2.3 Preparation of poly(DMAEMA)-grafted EVAL membrane

The poly(DMAEMA)-grafted EVAL membrane was prepared using UV-induced graft polymerization, as detailed in our previous publication.[30] Firstly, the EVAL membrane was washed by ethanol for 24 h to remove the impurities and additives. Then, EVAL membrane was dried and pre-coated in 50 mL solution with 5 g L^{-1} BP in acetone for 2 h. Secondly, BP-adsorbed EVAL membrane was placed between two pieces of quartz plate, immersed in DMAEMA solution and irradiated under UV light. The grafted membrane was subsequently extracted with ethanol by Soxhlet extraction for 48 h to remove redundant DMAEMA monomer and poly(DMAEMA) homopolymer. The grafting degree (GD) was calculated as follows:

$$\mathrm{GD} = \frac{m - m_0}{m_0} \times 100\% \quad (1)$$

where m_0 and m are the dry mass of the original and the poly(DMAEMA)-grafted EVAL membrane. The original and grafted EVAL membrane (GD 5%, 10% and 15%) were expressed as $EVAL_0$, $EVAL_5$, $EVAL_{10}$ and $EVAL_{15}$, respectively.

2.4 Morphology of membranes

The surface morphology of the membranes was examined by a field emission electron microscopy (FE-SEM, Hitachi S-4800, Japan). The accelerating voltage used was 10 kV. Samples of the membranes were attached with double-sided tape to steel stabs and sputter-coated with gold prior to FE-SEM measurements.

2.5 Zeta potential measurements

The effective surface charge characteristics of the membranes were evaluated from zeta potential measurements using a SurPASS electrokinetic analyzer (Anton Parr GmbH, Austria). The membrane was placed in an adjustable gap cell and filled with 10 mM KCl solution. The gap height was set to 100 μm and the pressure was varied between 0–300 mbar. The pH was adjusted with a 0.1 M HCl solution or a 0.1 M NaOH as needed. Each membrane was measured twice at each direction. The zeta potential (ξ) was calculated using the Helmholtz–Smoluchowski equation:

$$\xi = \frac{\mathrm{d}U}{\mathrm{d}p} \frac{\eta}{\varepsilon \varepsilon_0} \kappa_\mathrm{B} \quad (2)$$

where U is the stream potential, p is the pressure across the membrane, η is the viscosity of the electrolyte solution, ε is the dielectric constant of the electrolyte, ε_0 is the vacuum permittivity and κ_B is the electrolyte conductivity.

2.6 Static protein adsorption

2.6.1 Protein adsorption at different pH values. BSA solution was prepared in 10 mM phosphate buffer (PBS) with initial concentration of 1 mg mL^{-1}. The membrane was incubated in 10 mL BSA solution for 24 h in a shaker bath at 25 °C. Subsequently, the membrane was removed from the glass bottle and the BSA equilibrium concentration was measured by UV-VIS spectrophotometer (UL2100, GE, USA) with UV detection at 280 nm.

Adsorption capacity (Q_e) was calculated by eqn (3) as follows:

$$Q_e = \frac{(C_0 - C_e)V}{m} \quad (3)$$

where C_0 (mg mL^{-1}) is the BSA initial concentration and C_e (mg mL^{-1}) is the BSA equilibrium concentration, V (L) is the volume of the solution and m (g) is the dry mass of the membrane.

The effect of pH (3.6, 4.8, 6.4, 7.4, and 9.0) on the adsorption capacity was measured. The pH value was measured by using a pH meter (EL20, Mettler Toledo, Switzerland).

2.6.2 Adsorption isotherm. The adsorption isotherm was measured for BSA adsorption on the poly(DMAEMA)-grafted EVAL membrane. BSA concentration was 0.1, 0.2, 0.4, 0.6, 1.0, 1.5 and 2.0 mg mL^{-1} in 10 mM PBS at pH 6.4. Langmuir isotherm model and Freundlich isotherm model were adopted.

Langmuir isotherm model:

$$Q_e = \frac{Q_m C_e}{K_L + C_e} \quad (4)$$

where Q_e is the equilibrium adsorption capacity (mg g^{-1}), C_e is the equilibrium concentration (mg mL^{-1}), and K_L is the equilibrium constant (mL mg^{-1}). Q_m is the maximum adsorption capacity using a curve fitting (mg g^{-1}).

Freundlich isotherm model:

$$Q_e = K_F C_e^{1/n} \quad (5)$$

where Q_e and C_e have the same definitions as before; K_F and n are the Freundlich constants.

2.6.3 Adsorption kinetics. The kinetic experiment was performed at pH 6.4 with the initial BSA concentration of 1 mg mL^{-1}. The pseudo-first-order equation and the pseudo-second-order equation were adopted.

The pseudo-first-order model:

$$\lg(Q_e - Q_t) = \lg Q_e - \frac{k \times t}{2.303} \quad (6)$$

The pseudo-second-order model:

$$\frac{t}{Q_t} = \frac{1}{k_2 \times Q_e^2} + \frac{t}{Q_e} \quad (7)$$

where Q_e and Q_t are the adsorption capacity at equilibrium and at any time t, respectively (mg g^{-1}). k_1 and k_2 are the rate constants of the kinetic models.

2.7 Dynamic adsorption and desorption

Dynamic adsorption and desorption of poly(DMAEMA)-grafted EVAL membrane was measured using a custom-made dead-end filtration cell (Fig. 1). A total internal volume of the test cell was 10 mL and an effective membrane area was 15.9 cm^2. Two membranes were packed into the stack holder to form membrane stack. The feed-side pressure was maintained by a peristaltic pump (BT100-2J, Baoding Longer Precision Pump Co., Ltd.).

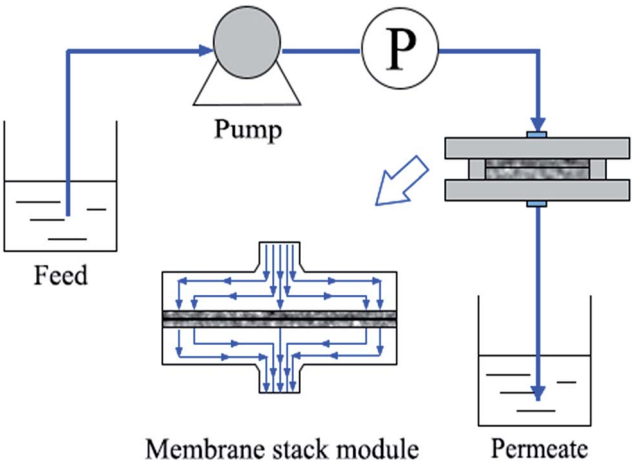

Fig. 1 Schematic diagram of experimental apparatus of dynamic protein adsorption.

Buffer A (10 mM PBS, pH 6.4) and buffer D (10 mM PBS, pH 9.0) were used as adsorption and desorption buffer, respectively. A typical protocol for a single run was as follows: (1) the cell was initially filled with buffer A and 60 mL buffer A was used to equilibrate membranes, (2) 0.6 mg mL^{-1} BSA solution was loaded through the stack holder at the flow rate of 3.8–28.3 L m^{-2} h^{-1}, (3) un-adsorbed BSA was washed from membrane stack with buffer A, (4) bounded BSA was eluted with buffer D until a stable baseline was observed. After each procedure, the cell was emptied and filled the solution of the next step. The permeate solution was collected and the BSA concentration was measured at 280 nm as previously described. The dynamic binding capacities were calculated at 10% and 50% breakthrough ($Q_{10\%}$ and $Q_{50\%}$).

The mass of desorbed BSA from the membrane was calculated from the area under the elution peak. Desorption efficiency was calculated as the quotient of the mass of desorbed BSA in elution to the mass of adsorbed BSA on the membrane, multiplied by 100%.

3. Results and discussion

3.1 Morphology of membranes

The poly(DMAEMA)-grafted EVAL membrane was prepared using UV-induced graft polymerization in our previous work. Surface composition, morphology and alkali-responsive properties (*i.e.*, contact angle, permeability, and selectivity) of the membrane were observed. The GD of membranes was obtained by varying the grafting condition, including initial BP concentration, UV irradiation time and monomer concentration. In this work, the original EVAL membrane with micron-sized membrane pore was used for preparing poly(DMAEMA)-

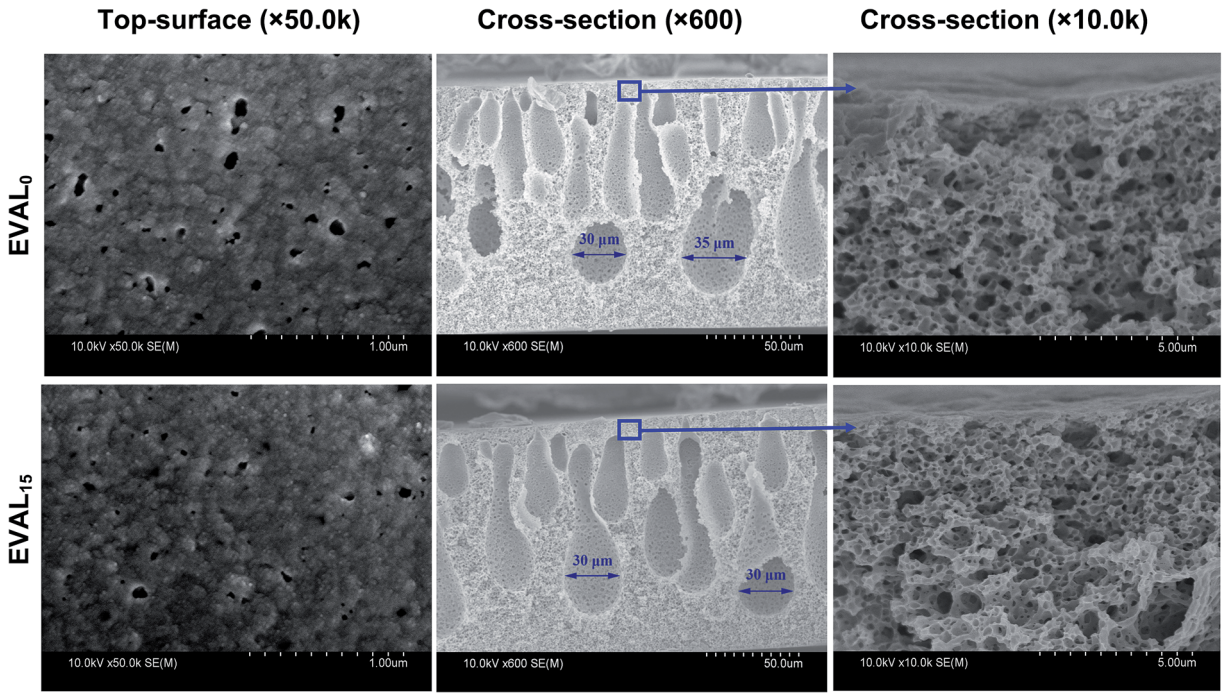

Fig. 2 FE-SEM images of the original and the poly(DMAEMA)-grafted EVAL membrane.

grafted EVAL membrane. The morphology of the membranes is presented in Fig. 2. The micron-sized membrane pores were observed on the membrane surface. The maximum pore size was approximately 0.1 μm–0.2 μm, the BSA molecule dimension was 8.0 × 8.0 × 3.0 nm,[33] thus the BSA molecule could permeate through the pore channels of the EVAL membrane freely. Both of the original and the poly(DMAEMA)-grafted EVAL membrane displayed high pore interconnectivity. Such membrane structure provided an interconnected path for convective flow in the adsorption process. After grafting polymerization, the membrane pores were narrowed, but the membrane pore morphology was intact.

3.2 Zeta potentials

The effect of pH on zeta potentials of the original and the poly(DMAEMA)-grafted EVAL membrane is presented in Fig. 3. The zeta potential of membrane $EVAL_0$ was negative over the entire studied pH range, most likely due to the preferential adsorption of negative anions from the electrolyte solution.[34,35] In contrast, the zeta potentials of membranes $EVAL_5$, $EVAL_{10}$ and $EVAL_{15}$ significantly increased due to the presence of the poly(DMAEMA) chains on the membrane surface. The zeta potentials of the membranes were increased by decreasing pH.

This could be ascribed to protonation of the tertiary amine of the poly(DMAEMA) chains at lower pH. The pK_a value of membrane $EVAL_{10}$ was higher than that of $EVAL_5$ because the effective charge density on the membrane surface was improved by increasing GD. However, the pK_a values of $EVAL_{10}$ and $EVAL_{15}$ were similar, probably not all poly(DMAEMA) chains of $EVAL_{15}$ exposed on the membrane surface, thus the effective charge density on membrane surfaces of $EVAL_{15}$ was approximate to that of $EVAL_{10}$.

3.3 Static protein adsorption

3.3.1 pH-Responsive protein adsorption. BSA was used as a model protein to measure the static protein adsorption of the membranes at different pH values (Fig. 4). The adsorption capacity of the original EVAL membrane was lower than 5.6 mg BSA per g membrane. The adsorption capacities of the grafted membrane were significantly improved and a positive relationship of adsorption capacity with GD was observed. It is because higher GD means higher densities of poly(DMAEMA) chains, which could serve as more sites for protein adsorption.

As shown in Fig. 4, the effect of pH on adsorption capacity was significant. The maximum BSA adsorption capacity was

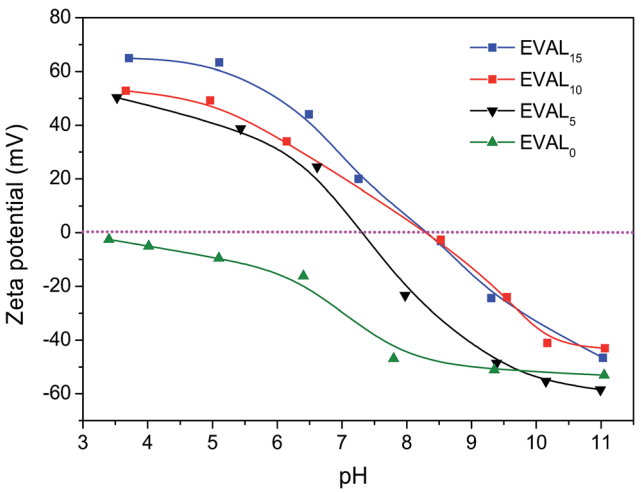

Fig. 3 The effect of pH on zeta potentials of the original and the poly(DMAEMA)-grafted EVAL membrane.

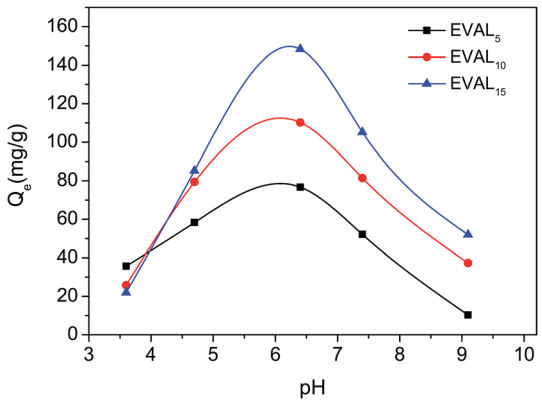

Fig. 4 The effect of pH on static protein adsorption of poly-(DMAEMA)-grafted EVAL membrane (1 mg BSA per mL, 10 mM PBS).

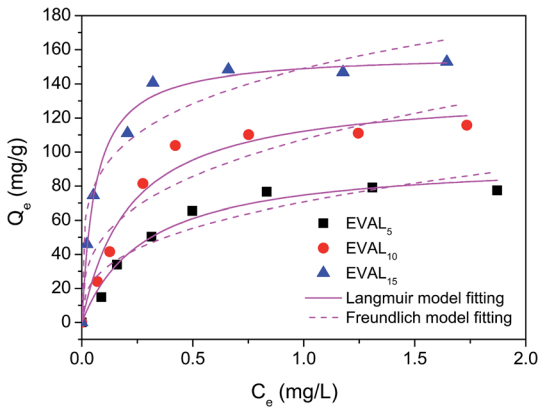

Fig. 5 Adsorption isotherms of protein adsorption on the poly-(DMAEMA)-grafted EVAL membrane (pH 6.4, 10 mM PBS).

obtained at pH 6.4. The poly(DMAEMA)-grafted EVAL membrane surface was positively charged at pH 6.4, while the BSA molecule (pI 4.7–4.9) was negatively charged. Thus, electrostatic interaction led to significant BSA adsorption. At pH 3.6, very weak BSA adsorption was observed because of charge repulsion. When pH was 9.0, the positive charge of membrane surface disappeared due to the deprotonated of grafted chains, thus the BSA adsorption capacity was low. The above results demonstrated that the BSA adsorption could be tuned by varying pH value. In static adsorption process, protein adsorption mainly depended on electrostatic behavior between grafted chains and protein. In this case, pH 6.4 was selected for BSA adsorption.

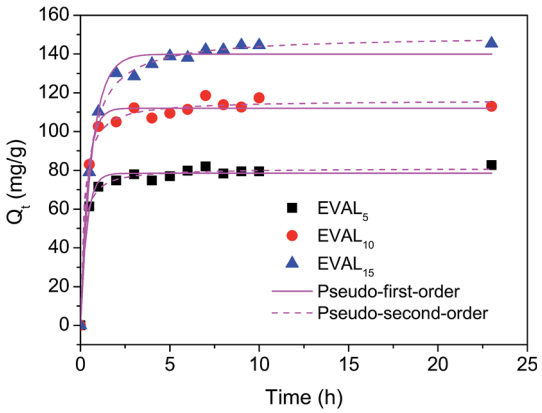

Fig. 6 Adsorption kinetics of protein adsorption on the poly-(DMAEMA)-grafted EVAL membranes (1 mg BSA per mL, pH 6.4, 10 mM PBS).

3.3.2 Adsorption isotherm. The BSA adsorption isotherms on the poly(DMAEMA)-grafted EVAL membrane are shown in Fig. 5 and the fitting parameters are given in Table 1. The BSA adsorption capacity of the membranes increased with increasing the initial concentration and GD. The experimental data were well fitted to the Langmuir type, suggesting that a monolayer of BSA molecule is adsorbed on the membrane surface. The maximum adsorption capacity of the poly(DMAEMA)-grafted EVAL membrane was 157.8 ± 4.0 mg BSA per g membrane. The electrostatic interaction between charged BSA molecule and tertiary amine groups of poly(-DMAEMA) chain plays an important role in protein adsorption. It is interesting to see how many tertiary amine groups adsorbed per BSA molecule. From the adsorption isotherm data of $EVAL_{15}$ (0.15 g poly(DMAEMA) per g membrane; 0.16 g BSA per g membrane), the mass ratio of DMAEMA and BSA was 0.94; the relative molecular mass ratio of DMAEMA and BSA was 2.35×10^{-3}. Thus, the molar ratio of DMAEMA and BSA was about 400, indicating that 400 tertiary amine groups involved in adsorption of per BSA molecule.

3.3.3 Adsorption kinetics. The BSA adsorption kinetics of poly(DMAEMA)-grafted EVAL membranes are presented in Fig. 6, and the parameters are shown in Table 2. Two kinetic models were well-described BSA adsorption on the membrane, especially, the pseudo-second-order adsorption kinetic model with $R^2 > 0.99$. The results indicated that chemical interaction between the BSA molecule and the membrane dominated the overall adsorption rate.

Table 1 Adsorption isotherm fitting parameters of membranes

	Langmuir model			Freundlich model	
Membrane	Q_m (mg g^{-1})	K_L (L mg^{-1})	R^2	K_F (mg g^{-1})(L mg^{-1})$^{1/n}$	R^2
$EVAL_5$	96.2 ± 5.9	0.2889	0.9744	70.69	0.8964
$EVAL_{10}$	136.5 ± 9.3	0.2164	0.9634	107.45	0.8711
$EVAL_{15}$	157.8 ± 4.0	0.0603	0.9889	148.99	0.9279

Table 2 Kinetic parameters for protein adsorption of membranes

	Pseudo-first-order kinetic adsorption model			Pseudo-second-order kinetic adsorption model		
Membrane	k_1 (min^{-1})	Q_e (mg g^{-1})	R^2	K_2 (g (mg^{-1} min^{-1}))	Q_e (mg g^{-1})	R^2
$EVAL_5$	2.8781	78.5 ± 0.8	0.9865	3.38 × 10^6	81.2 ± 0.7	0.9941
$EVAL_{10}$	2.6208	112.1 ± 1.2	0.9860	8.62 × 10^6	116.2 ± 1.3	0.9904
$EVAL_{15}$	1.5653	139.9 ± 1.5	0.9874	8.36 × 10^6	149.5 ± 1.3	0.9956

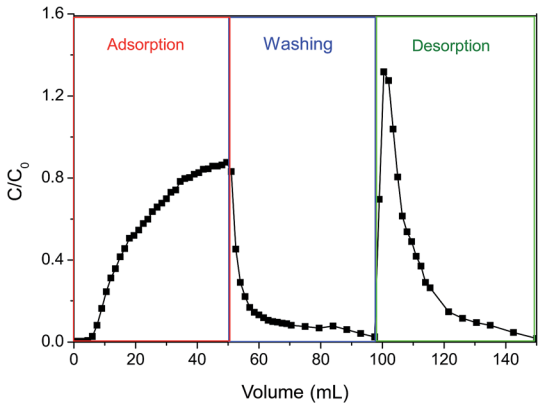

Fig. 7 The dynamic adsorption and desorption curve of poly(DMAEMA)-grafted EVAL membrane ($EVAL_{10}$, 0.6 mg BSA per mL, pH 6.4, 10 mM PBS, 3.8 L m^{-2} h^{-1}).

3.4 Dynamic protein absorption

3.4.1 The dynamic adsorption and desorption curve. During the dynamic absorption process, the unbound protein began to break through the membranes until the protein concentration in the effluent reached 87% of feed concentration. The unbound protein was washed with buffer A until the UV absorbance returned to its baseline. The $Q_{10\%}$ and $Q_{50\%}$ were 45 and 99 mg BSA per g membrane, respectively. The difference between $Q_{10\%}$ and $Q_{50\%}$ can be explained by the following two reasons: (1) the finger-like macrovoids with size of 30–35 μm within the membrane (cross-section of Fig. 2) caused inefficient utilization of the adsorption sites. (2) Membrane module design caused non-uniform flow distribution in the inlet (Fig. 1). The $Q_{50\%}$ of membrane $EVAL_{10}$ was equivalent to 22.6 mg BSA per mL of membrane, almost 95% of the static adsorption capacity (Fig. 7).

The bound protein was eluted with buffer D until a stable base-line was observed. The BSA was quickly desorbed from the membrane and 94% recovery of BSA was observed. The concentration of the eluted protein was 1.3-fold increase relative to the feed concentration. The electrostatic attraction between BSA and membrane surface disappeared and the poly(DMAEMA) chains were collapsed at pH 9.0. The high dynamic desorption efficiency at pH 9.0 depended on not only electrostatic behavior but also conformation change of pH-responsive chains. In addition, the effective pore size of the membranes increased when the poly(DMAEMA) chains were deprotonated, mass transfer resistance decreased, thus the dynamic desorption efficiency was improved.

The mechanism of protein adsorption and desorption on the pH-responsive EVAL membrane is shown in Fig. 8. The poly(DMAEMA) chains, which were grafted on the membrane surface and pore wall, acted as a pH sensor and a valve which regulated the protein adsorption and desorption properties of the membrane. Be differ from ion exchange membrane, electrostatic behavior is not the only factor for protein adsorption of pH-responsive membrane. The conformation change of grafted chains also plays an important role for pH-responsive protein adsorption and desorption. In this case, the transition of electrostatic behavior and conformation change of the poly(DMAEMA) chains both contributed to the pH-responsive protein adsorption and desorption. At pH 6.4, the grafted EVAL membrane surface was positively charged and the BSA molecule

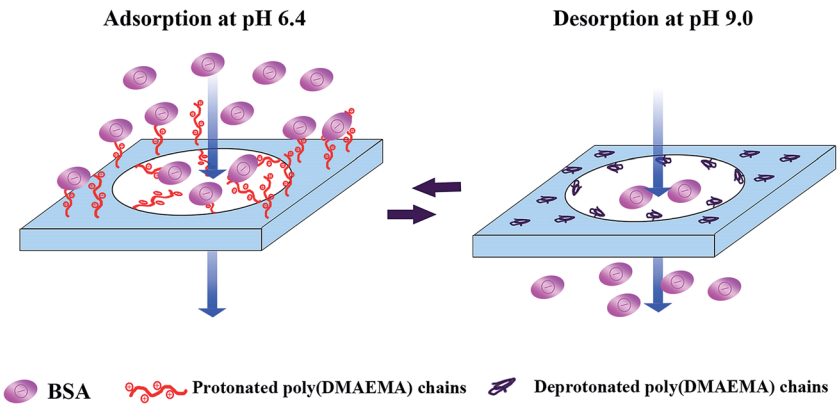

Fig. 8 pH-Responsive protein adsorption and desorption of the poly(DMAEMA)-grafted EVAL membrane.

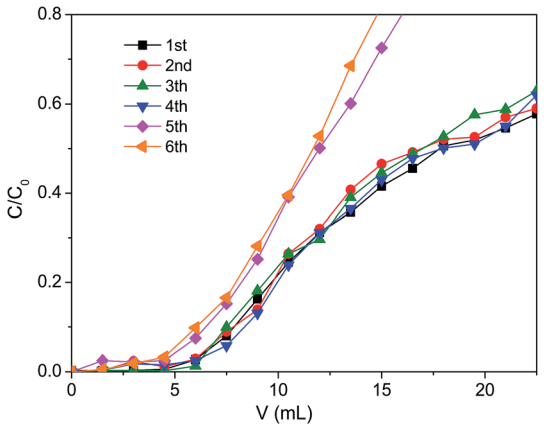

Fig. 9 The effect of adsorption/desorption cycle numbers on dynamic adsorption of membrane $EVAL_{10}$ ($EVAL_{10}$, 0.6 mg BSA per mL, pH 6.4, 10 mM PBS).

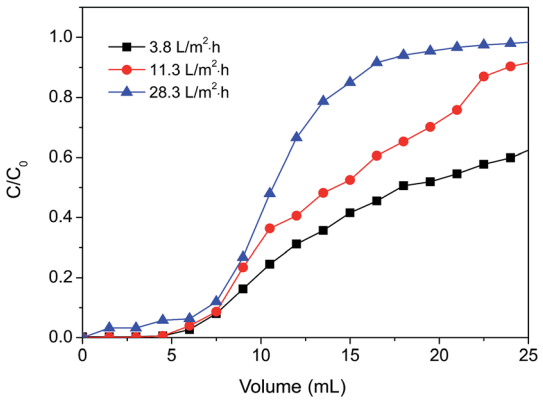

Fig. 10 The effect of flow rate on dynamic protein adsorption of poly(DMAEMA)-grafted EVAL membrane ($EVAL_{10}$, 0.6 mg BSA per mL, pH 6.4, 10 mM PBS).

was negatively charged. The significant BSA adsorption capability was obtained due to electrostatic interaction. Moreover, the protonated poly(DMAEMA) chains extended into the BSA solution in the filtration process, providing a three-dimensional space for BSA adsorption. The high dynamic desorption efficiency was obtained at pH 9.0 due to deprotonated and collapsed conformation of poly(DMAEMA) chains.

3.4.2 Reusability studies. The reusability of the membrane is an important aspect to evaluate its potential for large-scale application. After the described adsorption/desorption step, the membranes were washed with ultrapure water until neutral pH and reused in a next adsorption/desorption cycle without regeneration. The effect of adsorption/desorption cycles on breakthrough curves of the membranes are presented in Fig. 9. The $Q_{10\%}$ and $Q_{50\%}$ of membrane $EVAL_{10}$ for six adsorption/desorption cycles are presented in Table 3. The breakthrough curves and the dynamic adsorption capacities did not change after four sequential cycles. The breakthrough curves occurred earlier and the dynamic adsorption capacities decreased after the 5th adsorption/desorption cycle. The $Q_{10\%}$ decreased from 45 to 36 mg BSA per g membrane, and the $Q_{50\%}$ decreased from 99 to 72 mg BSA per g membrane.

3.4.3 Effect of flow rate. The transfer of BSA molecule to the adsorption sites though membrane is limited primarily by convection in filtration process. The residence time for BSA molecules through the membrane decreases by increasing flow rate. The effect of flow rate on breakthrough curves of the membranes is shown in Fig. 10. The dynamic capacities $Q_{10\%}$ and $Q_{50\%}$ are shown in Table 4. The breakthrough occurred earlier and the breakthrough curves became sharper by increasing the flow rate. The $Q_{10\%}$ and $Q_{50\%}$ decreased by increasing the flow rate and the $Q_{50\%}$ decreased more quickly.

Table 3 Dynamic adsorption capacities for sequential adsorption/desorption cycles of membrane $EVAL_{10}$

Cycle number	$Q_{10\%}$, mg BSA per g membrane	$Q_{50\%}$, mg BSA per g membrane
1st	45	99
2nd	45	99
3th	45	99
4th	45	99
5th	36	72
6th	36	72

Table 4 Dynamic adsorption capacities for different flow rates of membrane $EVAL_{10}$

Flow rate, L m^{-2} h^{-1}	$Q_{10\%}$, mg BSA per g membrane	$Q_{50\%}$, mg BSA per g membrane
3.8	45	99
11.3	45	81
28.3	36	63

4. Conclusions

Model protein BSA adsorption and desorption of the poly(DMAEMA)-grafted EVAL membrane with the interconnected porous structure was investigated. The maximum static BSA adsorption capacity was observed at pH 6.4. Fitted on Langmuir model the monolayer adsorption of BSA molecule on the membrane surface was found. The chemical interaction between the BSA molecule and the membrane dominated the overall adsorption rate. The dynamic adsorption capacity of membrane $EVAL_{10}$ at 10% and 50% breakthrough were 45 and 99 mg BSA per g membrane, respectively. The $Q_{50\%}$ of membrane $EVAL_{10}$ was equivalent to 22.6 mg BSA per mL of membrane, almost 95% of the static adsorption capacity. The BSA was quickly desorbed from the membrane and 94% recovery of BSA was observed at pH 9.0 in dynamic desorption process. The transition of electrostatic behavior and conformation change of the poly(DMAEMA) chains contributed to the pH-responsive protein adsorption and desorption. The dynamic adsorption capacity of the membrane did not change significantly after four sequential cycles. The breakthrough occurred earlier by increasing the flow rate and the dynamic capacity decreased.

Acknowledgements

This research was sponsored by the National Natural Science Foundation of China (Funding No. 51373120, 51503146), Science and Technology Commission Foundation of Tianjin (No. 15JCZDJC37600), and the Research Fund for the Doctoral Program of Higher Education (Funding No. 20111201110003). Program for Changjiang Scholars and Innovative Research Team in University (PCSIRT) of Ministry of Education of China (Grand No. IRT13084); The Science and Technology Plans of Tianjin (No. 15PTSYJC00240, 15PTSYJC00230).

References

1 V. Orr, L. Zhong, M. Moo-Young and C. P. Chou, *Biotechnol. Adv.*, 2013, **31**, 450–465.
2 A. Saxena, B. P. Tripathi, M. Kumar and V. K. Shahi, *Adv. Colloid Interface Sci.*, 2009, **145**, 1–22.
3 Y. Wei, J. Ma and C. Wang, *J. Membr. Sci.*, 2013, **427**, 197–206.
4 H. C. Chenette, J. R. Robinson, E. Hobley and S. M. Husson, *J. Membr. Sci.*, 2012, **432–424**, 43–52.
5 Y. Liu, Z. Feng, Z. Shao and X. Chen, *Mater. Sci. Eng., C*, 2012, **32**, 1669–1673.
6 M. He, C. Wang and Y. Wei, *RSC Adv.*, 2016, **6**, 6415–6422.
7 K. K. R. Tetala, K. Skrzypek, M. Levisson and D. F. Stamatialis, *Sep. Purif. Technol.*, 2013, **115**, 20–26.
8 N. Anuraj, S. Bhattacharjee, J. H. Geiger, G. L. Baker and M. L. Bruening, *J. Membr. Sci.*, 2012, **389**, 117–125.
9 N. Mustafaoglu, T. Kiziltepe and B. Bilgicer, *Analyst*, 2016, **141**, 6571–6582.
10 H. H. Himstedt, X. Qian, J. R. Weaver and S. R. Wickramasinghe, *J. Membr. Sci.*, 2013, **447**, 335–344.
11 Q. Wu, R. Wang, X. Chen and R. Ghosh, *J. Membr. Sci.*, 2014, **471**, 56–64.
12 C. Zhao, S. Nie, M. Tang and S. Sun, *Prog. Polym. Sci.*, 2011, **36**, 1499–1520.
13 Z. Liu, W. Wang, R. Xie, X.-J. Ju and L.-Y. Chu, *Chem. Soc. Rev.*, 2016, **45**, 460–475.
14 D. Wandera, S. R. Wickramasinghe and S. M. Husson, *J. Membr. Sci.*, 2010, **357**, 6–35.
15 M. Motornov, Y. Roiter, I. Tokarev and S. Minko, *Prog. Polym. Sci.*, 2010, **35**, 174–211.
16 Y. Stetsyshyn, K. Fornal, J. Raczkowska, J. Zemla, A. Kostruba, H. Ohar, M. Ohar, V. Donchak, K. Harhay, K. Awsiuk, J. Rysz, A. Bernasik and A. Budkowski, *J. Colloid Interface Sci.*, 2013, **411**, 247–256.
17 L. Mei, R. Xie, C. Yang, X.-J. Ju, J.-Y. Wang, Z. Zhang and L.-Y. Chu, *J. Membr. Sci.*, 2013, **429**, 313–322.
18 K. Z. Mah and R. Ghosh, *J. Membr. Sci.*, 2010, **360**, 149–154.
19 Y. Su and C. Li, *J. Membr. Sci.*, 2007, **305**, 271–278.
20 K. Nishinari, Y. Fang, S. Guo and G. O. Phillips, *Food Hydrocolloids*, 2014, **39**, 301–318.
21 J. Yang, J. Guo, X.-Q. Yang, N.-N. Wu, J.-B. Zhang, J.-J. Hou, Y.-Y. Zhang and W.-K. Xiao, *J. Food Eng.*, 2014, **143**, 25–32.
22 L. Voswinkel and U. Kulozik, *Procedia Food Sci.*, 2011, **1**, 900–907.
23 A. Arunkumar and M. R. Etzel, *J. Membr. Sci.*, 2015, **475**, 340–348.
24 X.-X. Yang, W. Gu, L. Liang, H.-L. Yan, Y.-F. Wang, Q. Bi, T. Zhang, J. Yu and G.-X. Rao, *RSC Adv.*, 2017, **7**, 3089–3100.
25 A. N. N. Murakami, R. D. d. M. C. Amboni, E. S. Prudêncio, E. R. Amante, C. B. Fritzen-Freire, B. C. B. Boaventura, I. d. B. Muñoz, C. d. S. Branco, M. Salvador and M. Maraschin, *Food Chem.*, 2013, **141**, 60–65.
26 M. E. Avramescu, W. F. C. Sager, M. H. V. Mulder and M. Wessling, *J. Membr. Sci.*, 2002, **210**, 155–173.
27 M. Avramescu, *J. Membr. Sci.*, 2003, **216**, 177–193.
28 S. M. Saufi and C. J. Fee, *J. Chromatogr. A*, 2011, **1218**, 9003–9009.
29 S. M. Saufi and C. J. Fee, *Sep. Purif. Technol.*, 2011, **77**, 68–75.
30 H. Ye, L. Chen, A. Li, L. Huang, Y. Zhang, Y. Li and H. Li, *J. Appl. Polym. Sci.*, 2015, **132**, 41775.
31 M. Liu, L. Zhao, S. Li, H. Ye, H. An and Y. Zhang, *RSC Adv.*, 2016, **6**, 10704–10712.
32 Y. Cai, J. Li, Y. Guo, Z. Cui and Y. Zhang, *Desalination*, 2011, **283**, 25–30.
33 D. H. Tsai, F. W. DelRio, A. M. Keene, K. M. Tyner, R. I. MacCuspie, T. J. Cho, M. R. Zachariah and V. A. Hackley, *Langmuir*, 2011, **27**, 2464–2477.
34 M. M. Rohani and A. L. Zydney, *J. Membr. Sci.*, 2012, **397–398**, 1–8.
35 M. Kumar and M. Ulbricht, *J. Membr. Sci.*, 2013, **448**, 62–73.